SUPPORTING INFORMATION

Targeting ligandable pockets on PHD zinc finger domains by a fragment-based approach

Anastasia Amato, Xavier Lucas, Alessio Bortoluzzi, David Wright and Alessio Ciulli*

Division of Biological Chemistry and Drug Discovery, School of Life Sciences, University of Dundee, James Black Centre, Dow Street, Dundee DD1 5EH, U.K.

* Corresponding author

Correspondence: Alessio Ciulli (a.ciulli@dundee.ac.uk)

EXPERIMENTAL SECTION

PROTEIN EXPRESSION AND PURIFICATION

Unlabelled and ^{15}N labelled BAZ2A and BAZ2B PHD were expressed and purified as previously described. [1, 2]

PEPTIDE SYNTHESIS

Peptides were synthesised on ResPep SL peptide synthesizer (Intavis) using standard automated solid-phase synthesis on a 24-column set up. The synthetic protocol included several cycles of deprotection, washing, coupling and washing. Each cycle started with Fmoc deprotection of the N–protected amino acid using 20% piperidine in DMF; a two steps coupling was then performed with 1 eq of 2-(1H-benzotriazol-1-yl)-1,1,3,3-tetramethyluronium hexafluorophosphate (HBTU) and 1 eq of 1-[Bis(dimethylamino)methylene]-1H-1,2,3-triazolo[4,5-b]pyridinium 3-oxid hexafluorophosphate (HATU). Unreacted amino acids were capped with a solution of 5% (v/v) acetic anhydride and N-methylmorpholine (NMM) in DCM. DCM solvent was used for the washing steps. Rink Amide AM resin (200-400 mesh) was used as solid phase. For the cleavage of the peptides from the resin a mixture containing 92.5% trifluoroacetic acid (TFA), 5% Triisopropylsilane and 2.5% water (v/v/v) was used. 100-150 mg of resin were incubated with 1 mL of cleavage mixture for 3h, as suggested by the manufacturer. Peptides were separated from the resin using a single-fritted column and precipitated in 5 ml of ice-cold diethyl ether. The resulting pellet was washed with diethyl ether and then dissolved in water and lyophilised in a centrifugal evaporator (Genevac EZ-2 series, SP Scientific).
Amino acids and resin used in the synthesis were purchased by Merck Millipore.

Peptide purification and analysis
Peptides were purified using high-performance liquid chromatography (HPLC) on a Gilson Preparative HPLC System with Waters X-Bridge C18 column (100 mm x 19 mm; 5 μm particle size) at 25 mL/min. A gradient in a range of 5–25% (v/v) acetonitrile in water supplemented with 0.1% (v/v) TFA was applied for the purification. All the peptides were eluted at the beginning of the gradient. VAriPure IPE column (Agilent) was used to remove TFA and ^{19}F NMR spectra confirmed the absence of TFA.
Analysis of the purified peptides was performed by LC-MS on Agilent Technologies 1200 series HPLC connected to an Agilent Technologies 6130 quadrupole LC/MS linked to an Agilent dioden array detector. Chromatographic runs were performed with a Waters X-Bridge C18 column (50 mm × 2.1 mm, 3.5 μm particle size) The chosen mobile phase was 5-95% water/acetonitrile plus 0.1% TFA over 3 min.

NMR SPECTROSCOPY

NMR experiments were performed using a AV-500 MHz Bruker spectrometer equipped with a 5 mm CPQCI-^{1}H-^{19}F/^{13}C/^{15}N/D Z-GRD cryoprobe.
All spectra were recorded and processed with TopSpin (Bruker) and analysed with CCPNMR software.

NMR fragment screening

^{15}N(^{1}H)-HSQC spectra of BAZ2 PHDs were recorded at ~100 μM for BAZ2A and ~150 μM for BAZ2B in 200 μL NMR buffer containing 25 mM $H_2PO_4^-$/HPO_4^{2-}, 50 mM KCl, 1 mM DTT and 20% D_2O at pH 6.9 and 6.5, respectively. Labelled proteins were then incubated with 5 mM of each fragment at final concentration of 1.25% of d_6-DMSO. Spectra of proteins incubated with fragment were overlaid with the spectrum of the *apo* protein containing 1.25% d_6-DMSO.

Chemical shift perturbations and K_D estimation

Chemical shift perturbation experiments were performed at the same protein concentration and pH as above but in 50 mM $H_2PO_4^-$/HPO_4^{2-}, 1 mM DTT and 20% D_2O. Each fragment was titrated in each protein at increasing concentration in a range between 0.5 mM and 5 mM. As reference spectrum was used the apo form.
The weighted chemical shift difference ($\Delta\delta_{weighted}$) was calculated using the equation:
$\Delta\delta_{weighted} = \sqrt{|\Delta\delta H|^2 + |\Delta\delta N|^2 * 0.15}$,[3] where $\Delta\delta H$ is the chemical shift on the proton and $\Delta\delta N$ is the chemical shift on the nitrogen which is scaled with a factor 0.15 to account for the different range of the amide proton and amide nitrogen. Chemical shifts for each backbone amide group were measured from the peak detected in *apo* form spectrum to the peak at the end of the titration.
K_D of binding for each fragment were estimated using the following equation [3] in the CCPNMR software:

$$\Delta\delta\, obs = \Delta\delta\, max \frac{\left\{ Kd + Pt + Lt - \sqrt{(Kd + Pt + Lt)^2 - 4Pt \times Lt} \right\}}{2[P]t}$$

[P]t and [L]t are the total concentration of protein and ligand; $\Delta\delta_{obs}$ is the observed shift in regard to the reference, while $\Delta\delta_{max}$ is the maximum shift obtained upon saturation and is extracted from the fitting.
K_D for each fragment was extrapolated as an average value of $K_D \pm$ s.e.m. of those resonances with $\Delta\delta > \overline{\Delta\delta} + \sigma$.

HSQC acquisition times were: 60 ms (^{15}N) and 120 ms (^{1}H).

BIOPHYSICAL ASSAYS

Isothermal titration calorimetry

(ITC) experiments were performed with the ITC200 micro-calorimeter (GE Healthcare) at 298 K stirring the sample at 750 rpm.

Before titration, BAZ2 PHD zinc fingers were dialyzed overnight against buffer containing 20 mM Tris, 200 mM NaCl, 1 mM TCEP (tris(2-carboxyethyl)phosphine) pH 8.0, using the D-tube dialyzer MWCO 3.5 KDa (Millipore).

Titrations were performed in direct mode titrating 3 mM peptide solutions into 120 μM protein solution loaded in the calorimetric cell. First injection was of 0.4 μL (subsequently discarded during data analysis) followed by 19 injections of 2 μL at 120 s time intervals. For each protein, at the end of this first titration, in order to reach saturation of binding, 20 further injections were performed, after removing the excess of solution from the cell.

A control experiment of peptide into buffer was performed. Data were fitted keeping the stoichiometry N fixed at 1. Dissociation constant K_D and the enthalpy of binding ΔH were obtained using the MicroCal ORIGIN software package.

Thermal shift assay (TSA)

Thermal shift experiments were performed using a 96-well PCR plate in CFX96 Touch Real-time PCR detection system (Biorad). Each well contained 40 μL reaction and the final conditions were: 2.5X Sypro Orange (Invitrogen Molecular Probes) and 10 μM protein in 100 mM MES, 50 mM NaCl, pH 6.0. Fragments were screened against both proteins at three different concentrations: 3 mM, 5 mM and 15 mM in 5% (v/v) DMSO (dimethyl sulfoxide). Each sample was run in triplicate.

The assay was conducted by increasing the temperature from 25 °C to 95 °C at a rate of 1 °C per minute and detecting fluorescence at the end of each interval. Fluorescence was plotted versus temperature and the melting temperature (Tm) was extrapolated from the fitting of the Boltzmann equation using the "DSF analysis" excel spreadsheet available at ftp://ftp.sgc.ox.ac.uk/pub/biophysics. The tabulated ΔTm values are the difference of the mean of three independent measurements ± propagated s.d.

AlphaLISA

AlphaLisa competition assays were developed using biotinylated BAZ2 PHD and H3 double mutant peptide (ARTAATARKS) synthetized with the additional Anti-FLAG epitope at the C-terminus plus an intermediate flexible linker in order to avoid steric hindrance (ARTAATARKS-TGGSGGSG-DYKDDDDK). The assay was set up in a 384-well plate (PerkinElmer) in 100mM HEPES buffer pH 7.5, 0.1% BSA and 0.02% CHAPS. Each well contained a final concentration of 10 nM protein, 160 nM AlphaLISA peptide, fragment at desired concentration in 4% (v/v) DMSO and 10 μgmL^{-1} of each AlphaLISA beads (Anti-

FLAG AlphaLisa acceptor beads and Streptavidin donor beads). Beads were cautiously added to the solution under low light conditions. The plate was incubated for one hour at room temperature before to be read on a PHERAstar FS plate reader (BMG Labtech) at laser excitation of 680 nm and filter set on emission light at 615 nm. BAZ2 PHDs were tested against eight different peptide or fragment concentrations in 1:5 serial dilution. Fitting of the data to extrapolate IC_{50} values of the dose-response curves was performed using the GraphPad Prism 6 (GraphPad Software).

X-RAY CRYSTALLOGRAPHY

Crystallization

Crystals of BAZ2A and BAZ2B PHD domains were obtained by mixing equal volume of protein and crystallisation buffer (2.2-2.4 M Na/K phosphate at pH 8.5). BAZ2A PHD was crystallized at 6.5–7 mg ml^{-1} and BAZ2B PHD at 5.5–6 mgml^{-1}. Crystals were left to grow at 18°C for at least two days.

Crystallization H3 3-mer peptide in complex with BAZ2A PHD finger
Crystals of the complex of BAZ2A PHD with H3 3-mer were obtained soaking overnight preformed *apo* BAZ2A PHD crystals in a solution containing 20 mM H3 3-mer (ART) in crystallization buffer.

Crystallization H3 10-mer AA mutant peptide in complex with BAZ2A PHD finger

Crystals of the complex of BAZ2A PHD with H3 10-mer AA mutant peptide (ARTAATARKS) were obtained soaking overnight preformed apo BAZ2A PHD crystals in a solution containing 2.5 mM H3 10-mer in crystallization buffer.

Crystallization of Fr19 and Fr23 in complex with BAZ2A PHD finger

Crystals of the complex of BAZ2A PHD with Fr**19** and Fr**23** were obtained soaking for 24 h apo form crystals of BAZ2A in 10 µL of a solution containing crystallization buffer supplemented, respectively, with 50 mM Fr**19** and 50 mM Fr**23**.

Crystallization of Fr21 and Fr23 in complex with BAZ2B PHD finger

Crystals of BAZ2B PHD in complex with Fr**21** and Fr**23** were obtained soaking for 24h BAZ2B apo form crystals in a solution of crystallization buffer supplemented, with, respectively, 20 mM Fr**21** and 50 mM Fr**23**.

All the crystals, before to be flash-frozen, were cryo-protected in the soaking solution supplemented with 20% glycerol. All the fragments used were soluble in water up to 500 mM.

Data collection and structure determination

Data collections were performed at the beamlines at the Diamond Light Source (Didcot, UK) synchrotrons. Images of BAZ2A PHD crystals were indexed and integrated using XDS. [4, 5] Images of BAZ2B PHD were indexed and integrated using Mosflm.[6] Scaling and merging was performed using Aimless [7] from the CCP4i package and copying R free flags from the apo form pdb models used for the refinement (PDB: 4QF2 for BAZ2A and 4QF3 for BAZ2B). Structures were solved using 4QF2 pdb as model for BAZ2A and 4QF3 pdb as model for BAZ2B. Several rounds of refinement were performed using Refmac5[8] with TLS groups generated via TLSMD server. [9] F_o-F_c map showed clear electron density in the histone pocket to fit peptides and fragments. Waters were manually added to the model at the latest stages of the refinement before to model the ligands. Residues at the N-terminus of the protein chains were not visible, consequently they were not modeled. Modeling of the fragments was performed using the ligand builder in Coot. [10] The topology files of the fragments were generated using PRODRG2 server. [11] The quality of the models was checked by MolProbity, [12] and all structure figures were generated using PyMOL (The PyMOL Molecular Graphics System, Version 1.7.05, Schrödinger, LLC).

COMPUTATIONAL METHODS

Computational druggability assessment of BAZ2A PHD

The crystal structure of *apo* PHD of BAZ2A (PDB code 4QF2) was subjected to computational druggability assessment using FTMap.[13, 14] Water and solvent molecules present in the structure were removed in advance. Then, identified potential binding sites were classified according to their perceived druggability using the "classify_druggability" tool included in FTMap. Physicochemical properties of the pockets were examined using SiteMap v3.8 (Schrödinger Inc., LLC).

Virtual screening cascade of BAZ2A and BAZ2B PHDs

We assembled a diverse virtual library of a thousand commercially-available fragments and low-molecular weight biomimetics, peptidomimetics, and charged compounds. The molecules were processed using LigPrep v3.7 (Schrödinger Inc., LLC), and the protonation states were perceived using Epik 3.5 (Schrödinger Inc., LLC). The crystal structures of *apo* PHD of BAZ2A and BAZ2B (PDB codes 4QF2 and 4QF3, respectively) were subjected to molecular docking using Glide v7.0 (Schrödinger Inc., LLC). Water and solvent molecules present in the protein crystal structures were removed, and the proteins were prepared for docking using the Protein Preparation Wizard (Schrödinger Inc., LLC). Amino acid protonation states were assigned using PROPKA 3.0.[15, 16] Two grids were prepared for each of the prepared proteins: one covering the histone tail pocket, and another one centred in the newly proposed binding site at the back of the proteins. Each grid was used to screen virtually the compound library using the Standard Precision algorithm in Glide. The virtual screening results were normalized for ligand efficiency by dividing the docking score by the

number of heavy atoms in the molecule. Compounds with a normalized docking score ≥ 0.25 were redocked using the eXtra Precision (XP) algorithm in Glide. XP docking scores were again normalized by number of heavy atoms, and the top 200 compounds were subsequently processed with the MM-GBSA protocol in Prime 3.0 (Schrödinger Inc., LLC), considering water solvation and a protein shell of 5.0 Å surrounding the docked compounds as flexible with constraints.

Compound selection

Physicochemical properties and aqueous solubility of top-ranked compounds for each grid in terms of normalized docking score or normalized MM-GBSA E_{bind} were predicted using QikProp 4.7 (Schrödinger Inc., LLC) and the Calculator Plugins included in Marvin 15.9.7, 2015, ChemAxon (http://www.chemaxon.com). Surviving compounds (predicted pK_s ≤ 3) were visually inspected and a varied set of the most promising compounds was purchased for experimental validation of binding affinity.

Selection of Fr19 derivatives

We assembled a focused virtual library of commercially-available low-molecular weight compounds extracted from the ZINC 15 database.[17] We selected compounds containing the peptidic backbone of Fr**19** using the SMARTS pattern "[N;A;+1][C;A]C(=O)[#7]", which was generated informed by the crystal structure of BAZ2A in complex with the fragment and with assistance of SMARTSviewer. [18] Filtering of the compounds by having at least 1 aromatic ring (using Open Babel [19]) and a predicted pK_s ≤ 3 resulted in 4,196 unique molecules. Compound library preparation was carried out as above.

The histone pocket of the crystal structure of BAZ2A in complex with Fr**19** was subjected to the previously described molecular docking protocol to screen the focused compound library. Visual inspection of top-ranked hits based on MM-GBSA $E_{binding}$ led to the final selection of most promising compounds for purchase and experimental validation of binding affinity.

Torsion analysis of model compounds

Model compounds thiazolacetamide and phenylacetamide were subjected to fully flexible torsion analysis of their arylacetamide bond using DFT at the PBF (water) MN15-L/aug-cc-pVTZ(-F) level of theory in Jaguar 9.7 (Schrödinger Inc., LLC). The torsion was gradually rotated from 0 to 180º in 10º steps, and no molecular symmetry was considered during the analysis. Natural bond order (NBO) analysis of the global energy minimum in thiazolacetamide was carried out using NBO 6.0 (http://nbo6.chem.wisc.edu), as implemented in Jaguar.

SUPPLEMENTARY FIGURES.

A

H3 3-mer vs BAZ2A PHD

H3 3-mer vs BAZ2B PHD

K_D: 2.3 mM

K_D: 1.2 mM
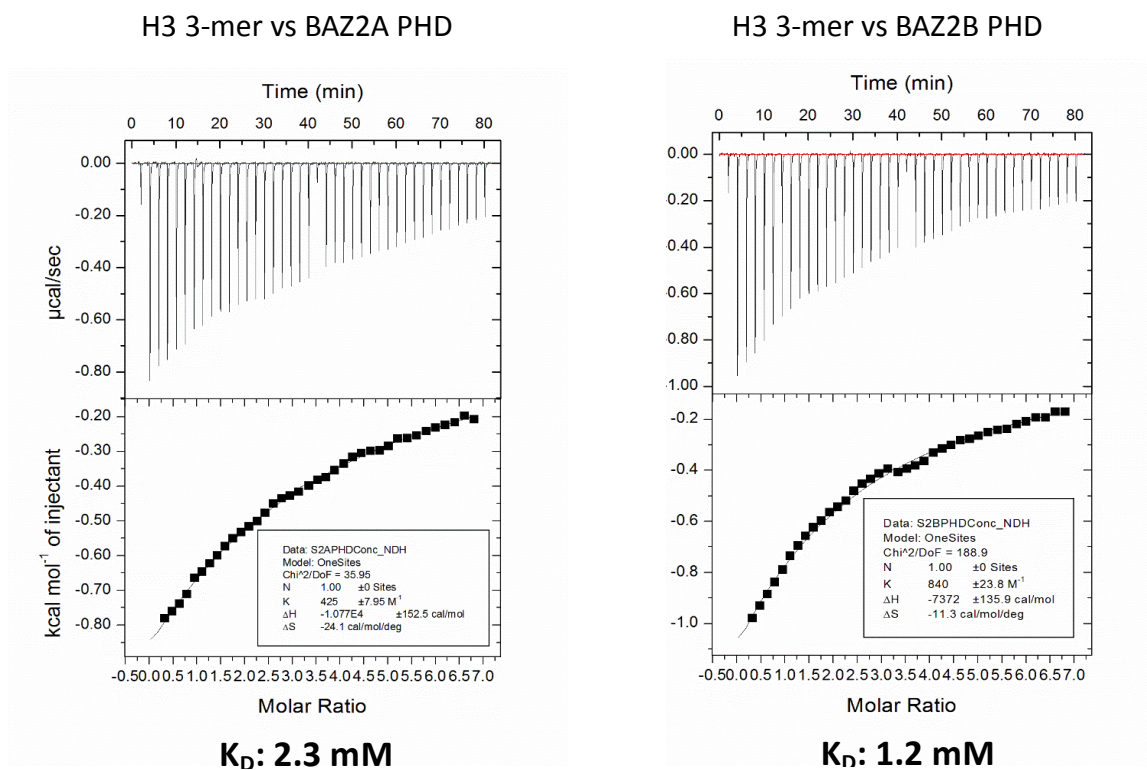
B
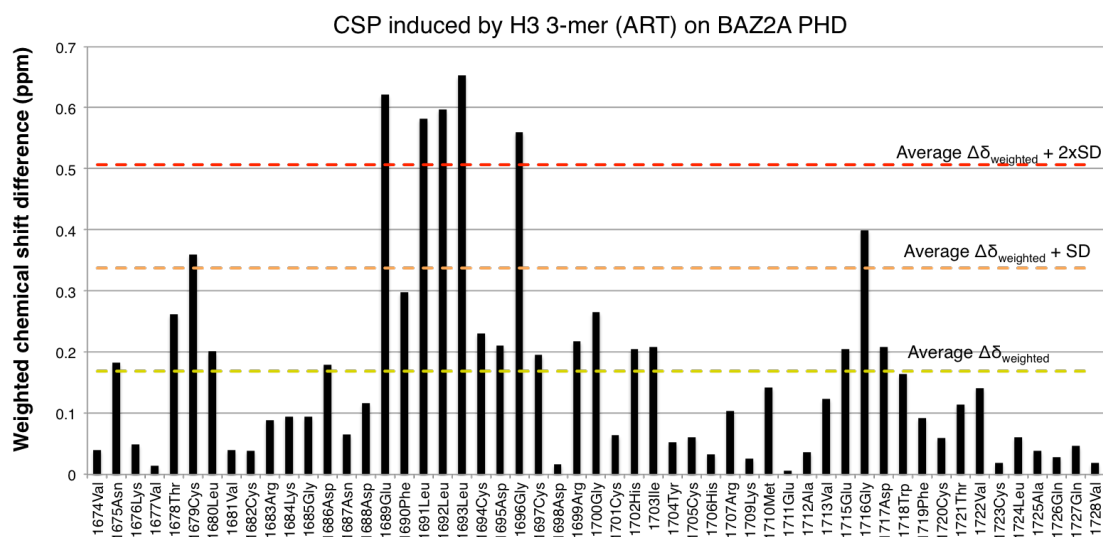
C
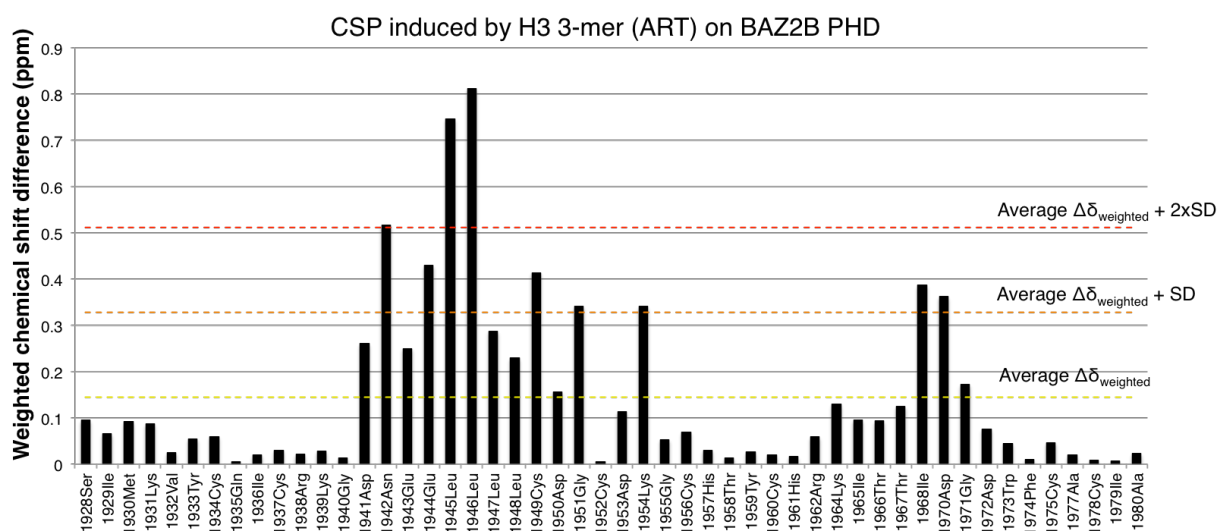
Figure S1 H3 3-mer peptide retains binding to BAZ2 PHDs. (A) ITC binding curves of H3 3-mer peptide titrated into BAZ2A and BAZ2B PHDs. In the upper panel, raw ITC data and in the lower panel, the integrated ΔH (kcal × mol^{-1}) are plotted against the peptide/protein ratio. Fitting of the data was obtained setting the N value as 1. K_D values are reported below each panel. (B) Histogram plotting the chemical shift perturbations induced by H3 3-mer peptide on BAZ2A PHD versus protein residues. Shifts are grouped according to their intensity: strong shifts (Δδ > $\overline{\Delta\delta}$ + 2σ), intermediate shifts (Δδ > $\overline{\Delta\delta}$ + σ) and weak shifts (Δδ > $\overline{\Delta\delta}$). (C) Histogram plotting the chemical shift perturbations induced by H3 3-mer peptide on BAZ2B PHD versus protein residues.
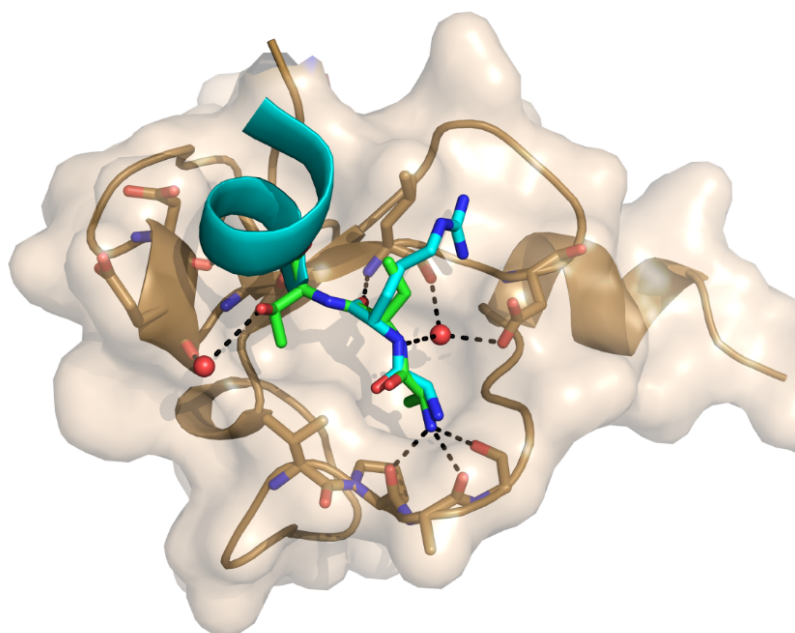
Figure S2. Superposition of PHD BAZ2A (wheat surface) in complex with H3 10-mer (cyan) and 3-mer peptide (green).
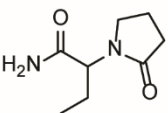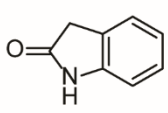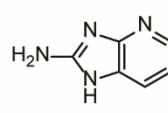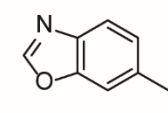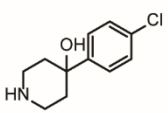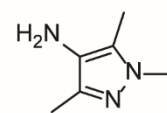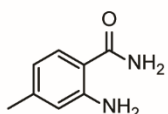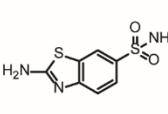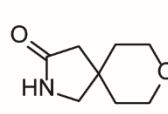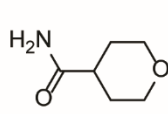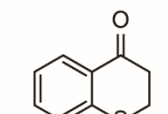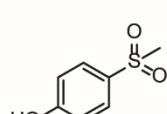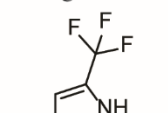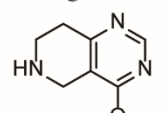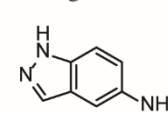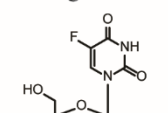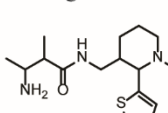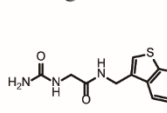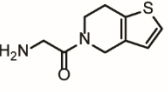
Table S1 Chemical structures of *in silico* fragment hits.

List of chemical structures of 19 fragments selected by docking. Fr**4** was not soluble in the assay conditions and therefore not tested.
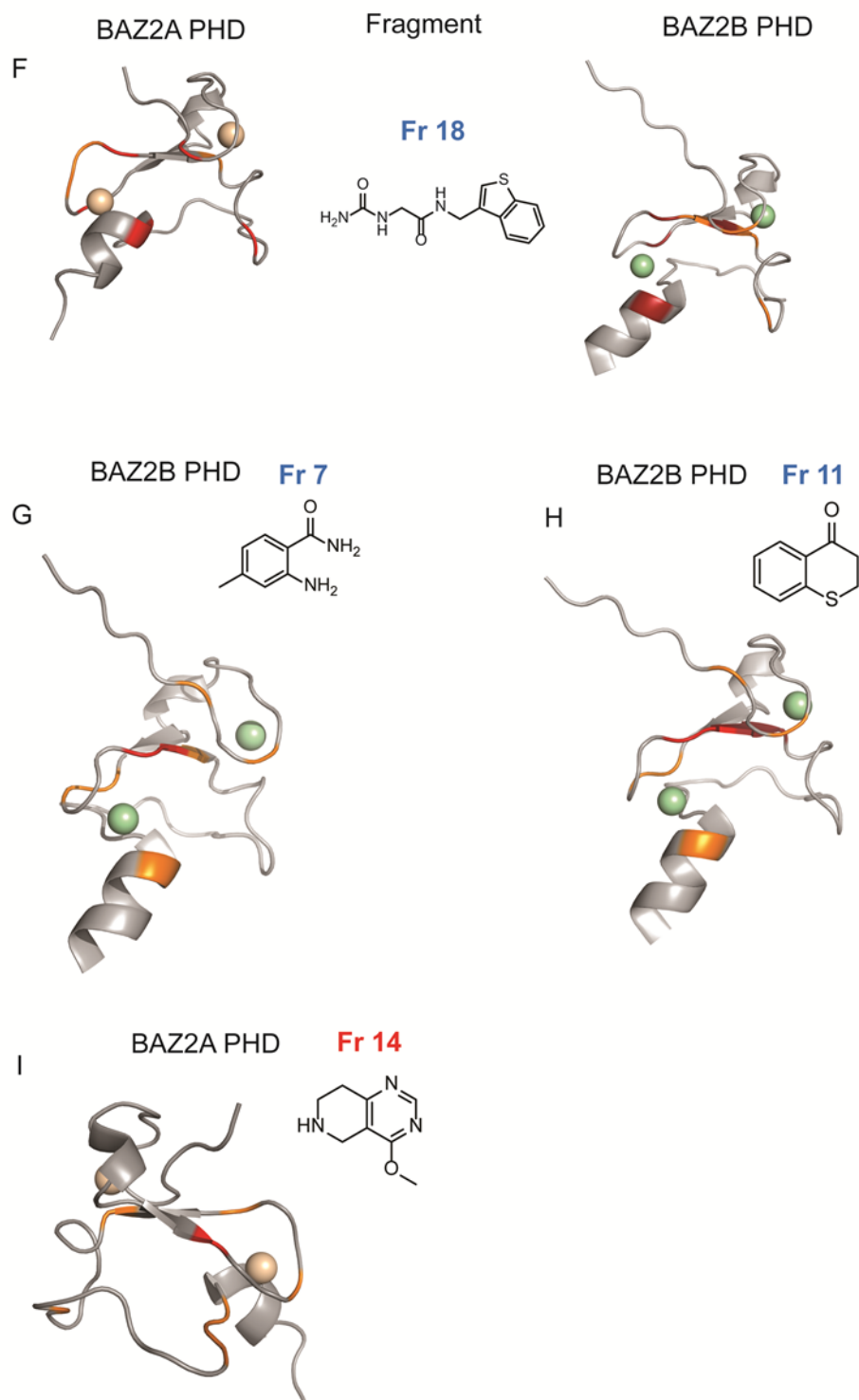
BAZ2A PHD   **Fragment**   **BAZ2B PHD**

A

Fr 3

B

Fr 5

C

Fr 8

D

Fr 17

E

Fr 19
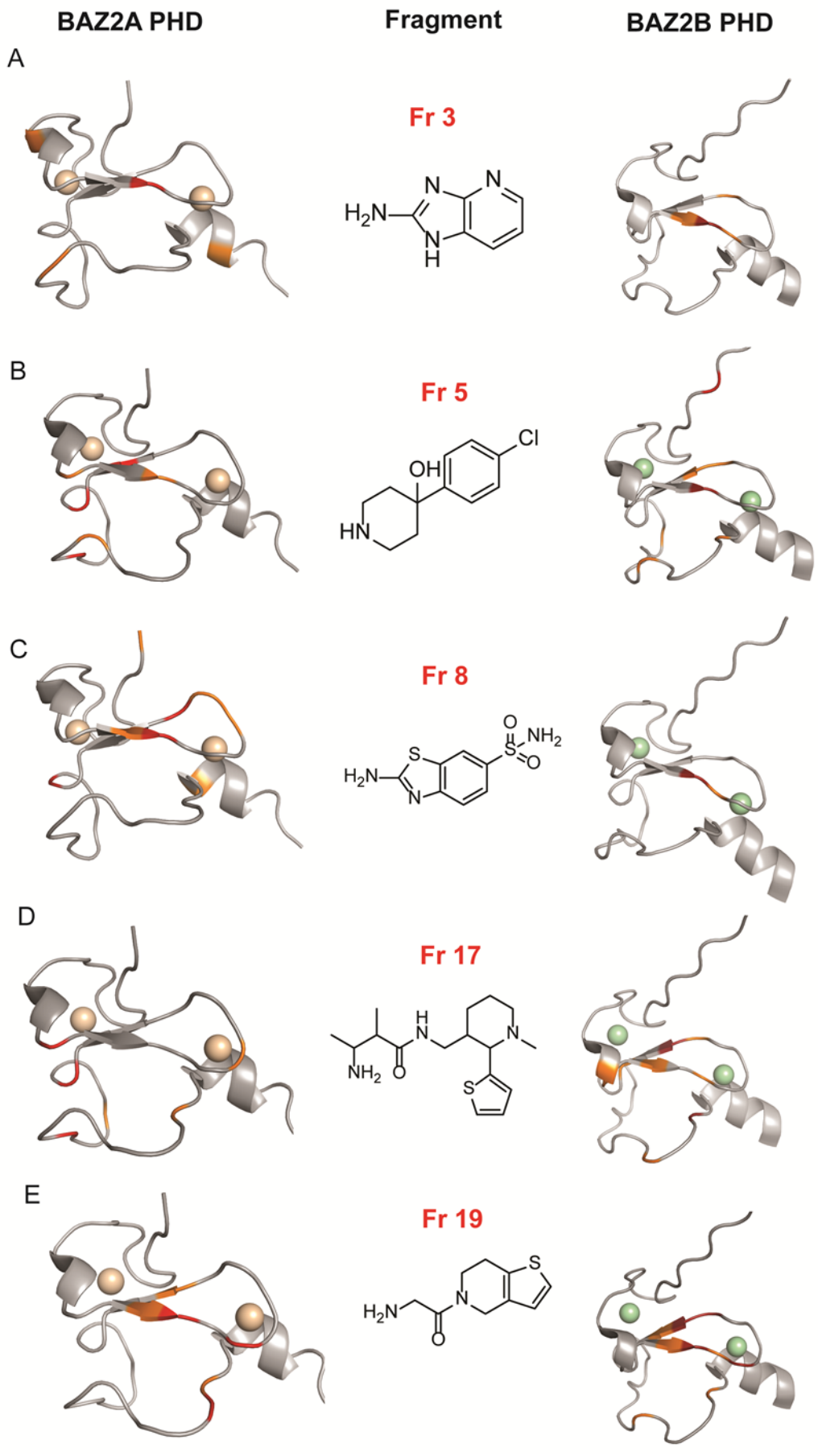
Figure S3. Heat maps of CSPs projected on BAZ2A/B PHDs.

CSPs induced by fragments (5 mM) and projected onto BAZ2A (PDB: 4QF2) and BAZ2B (PDB: 4QF3) PHDs. Residues were coloured according to the intensity of the shift: red for strong shifts ($\Delta\delta > \overline{\Delta\delta} + 2\sigma$), orange for intermediate shifts ($\Delta\delta > \overline{\Delta\delta} + \sigma$). In white all residues reporting intensity of shift $< \overline{\Delta\delta} + \sigma$. In red are fragments that reported shifts for the histone pocket, while in blue fragments that showed shifts for the "back-pocket".

Fragment	K_D (mM) BAZ2A PHD	K_D (mM) BAZ2B PHD
Fr**3**	NT	4.3 ± 1.3 (LE 0.36)
Fr**5**	4.7 ± 1.9 (LE 0.23)	>16 (LE 0.17)
Fr**8**	NT	4.4 ± 0.7 (LE 0.23)
Fr**14**	9.3 ± 1.6 (LE 0.23)	NT
Fr**17**	11 ± 2 (LE 0.13)	3.4 ± 0.3 (LE 0.16)
Fr**18**	9 ± 3 (LE 0.15)	2.3 ± 0.5 (LE 0.19)
Fr**19**	NT	9.4 ± 1.8 (LE 0.21)

Table S2.
K_D are calculated as mean ± s.e.m. of single K_D extrapolated from CSPs as described in the experimental section. In brackets, ligand efficiency in kcal × mol^{-1} × heavy atom^{-1}. NT = not tested.
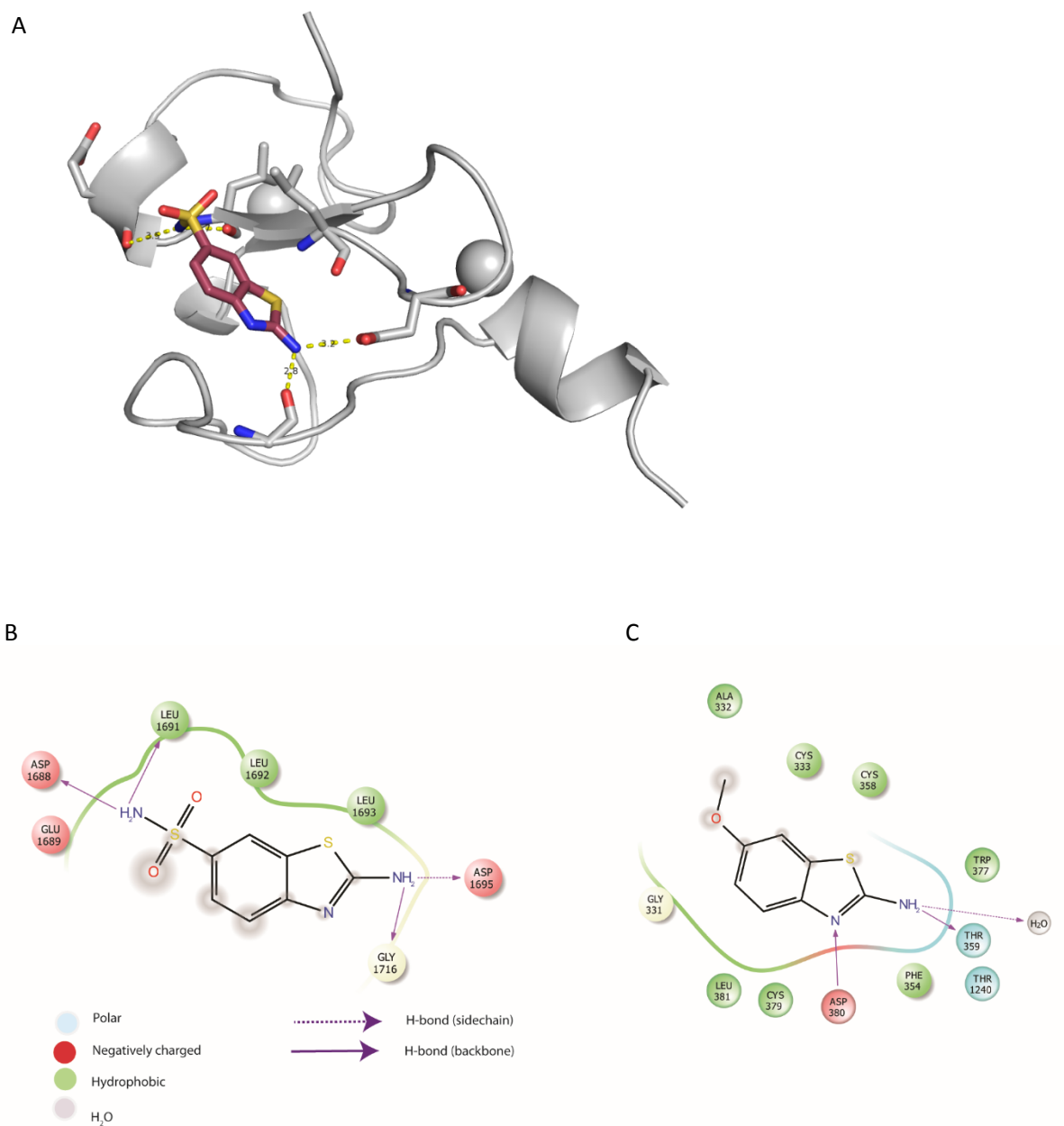
Figure S4. Binding pockets comparison.

(A) Docking pose of Fr**8** bound to BAZ2A PHD. (B) Ligplot[20] representation of docking pose of Fr**8** binding to the histone pocket in BAZ2A PHD (C) and Ligplot scheme of the crystal structure of CF4 binding to the benzothiazole cleft in Pygo PHD.[21] No similarities between the two pockets are observed and different binding mode is reported.
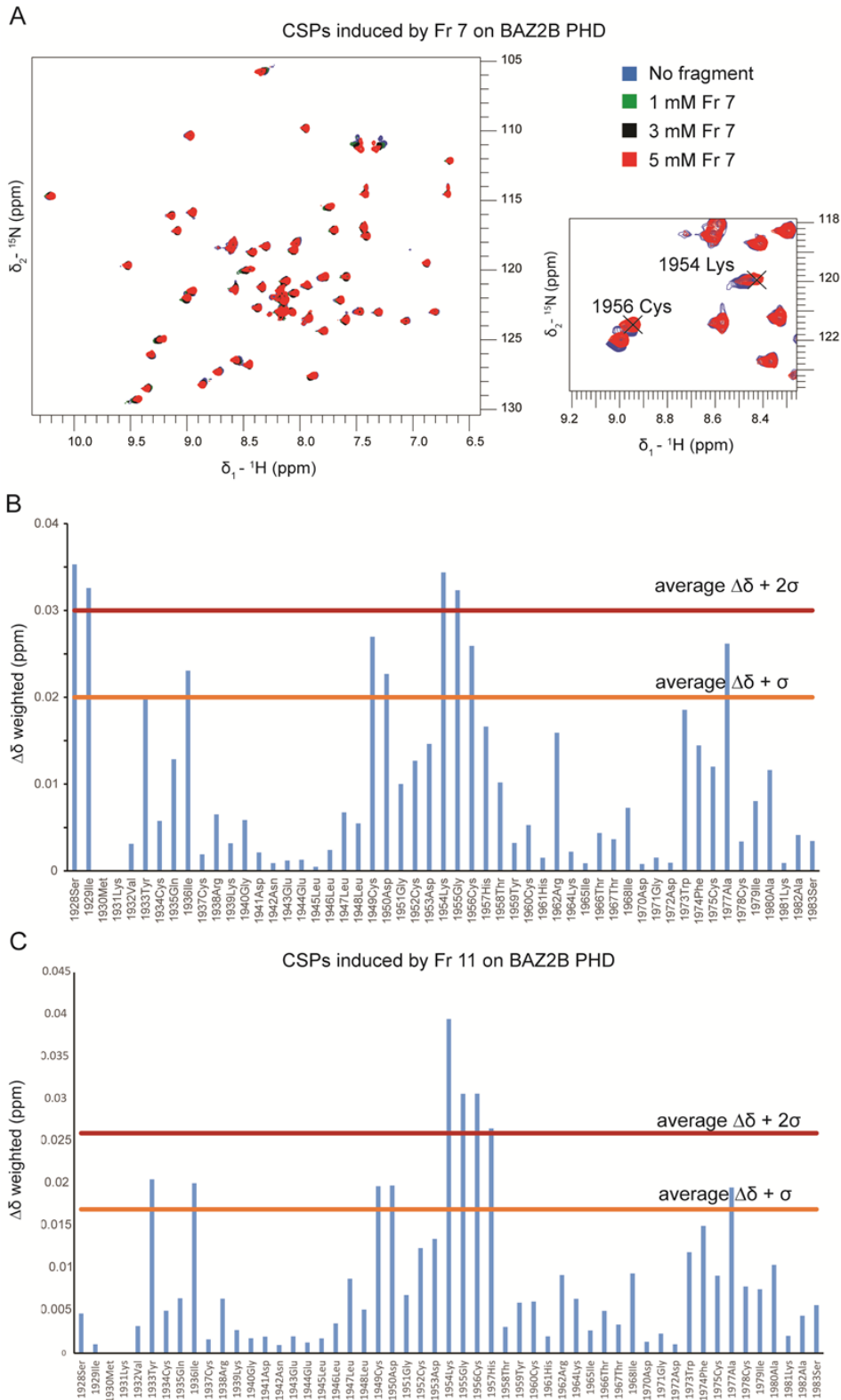
Figure S5 CSPs induced by Fr7 and Fr11.
(A) HSQC spectra showing titrations of PHD of BAZ2B with Fr**7**. Meaningful shifts are observed only at high fragment concentration (5 mM). (B) Histogram of weighted chemical shifts measured at 5 mM Fr**7** plotted against BAZ2B PHD protein sequence. (C) Histogram of weighted chemical shifts measured at 5 mM Fr**11** plotted against BAZ2B PHD protein sequence. For both fragments, the intensity of shifts is low ($\overline{\Delta\delta} + 2\sigma < 0.03$ ppm).
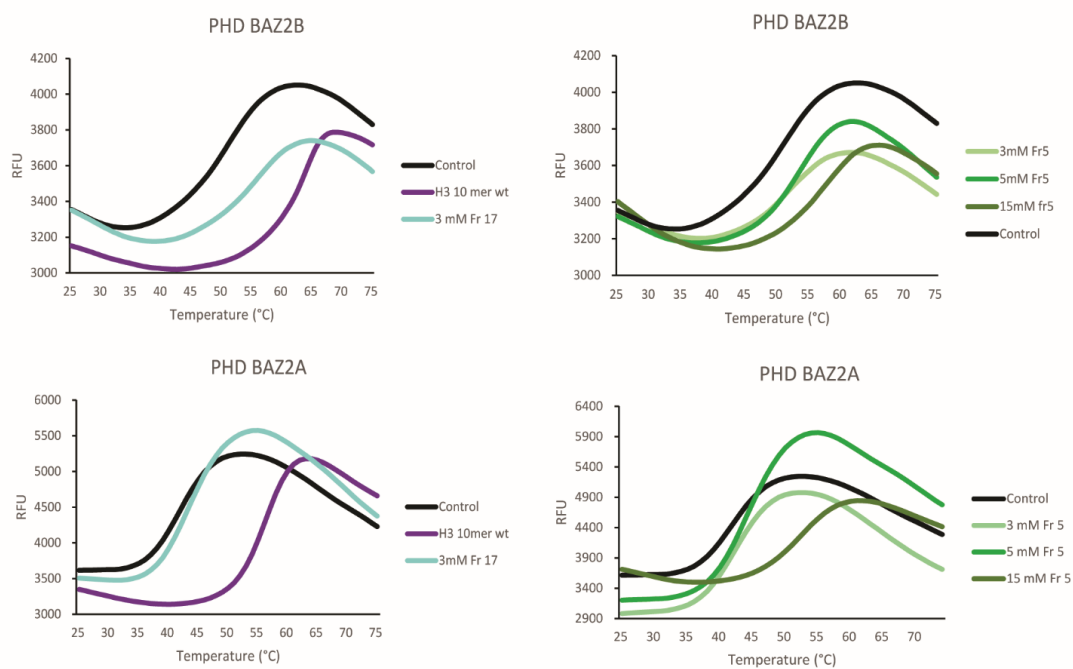
Figure S6 TSA melting curves of BAZ2 PHDs.
TSA melting curves of BAZ2 PHDs reported as relative fluorescence units (RFU) *versus* temperature (°C). Melting curves of the protein without any ligand are reported in black. On the left side, 500 µM H3 10-mer peptide (in purple) was used as positive control. In cyan, melting curves of PHDs in presence of 3 mM Fr**17**. On the right side, TSA melting curves of BAZ2 PHDs in presence of increasing concentrations of Fr**5**.
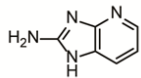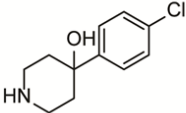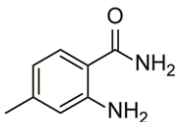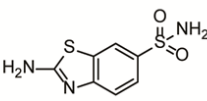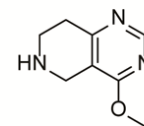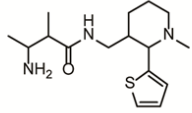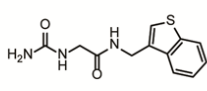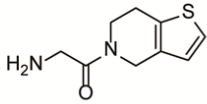
Ligand	ΔTm (°C) BAZ2A	ΔTm (°C) BAZ2B	[Compd]
H3 ARTKQTARKS*	14 ± 0.3	12 ± 0.6	500 µM
Fr3	ND	ND	3 mM 5 mM 15 mM
Fr5	1.3 ± 0.5 3.0 ± 0.7 9.8 ± 0.5	1.4 ± 0.6 2.3 ± 0.9 5.9 ± 1.4	3 mM 5 mM 15 mM
Fr7	NT	-0.9 ± 0.7 -1.9 ± 0.9 ND	3 mM 5 mM 15 mM
Fr8	ND	ND	3 mM 5 mM 15 mM
Fr14	1.2 ± 0.7 1.5 ± 0.3 1.9 ± 0.5	1.9 ± 0.9 2.2 ± 0.6 ND	3 mM 5 mM 15 mM
Fr17	2.2 ± 0.3 NT NT	4.9 ± 0.9 NT 13.9 ± 1.5	3 mM 5 mM 15 mM
Fr18	-1.7 ± 0.6 ND ND	ND	3 mM 5 mM 15 mM
Fr19	-1.4 ± 0.3 -0.9 ± 0.4 NT	0.5 ± 0.8 -2.2 ± 0.6 0.6 ± 0.6	3 mM 5 mM 15 mM
Fr2 non-binder	NT	-0.2 ± 0.7 -0.4 ± 0.7 -1.2 ± 0.7	3 mM 5 mM 15 mM
Fr13 non-binder	NT	0 ± 0.7 -1.4 ± 0.7 0.5 ± 0.8	3 mM 5 mM 15 mM

Table S3 List of ΔTm calculated by TSA.

List of the ΔT_m calculated by TSA for each protein upon addition of 3, 5 and 15 mM of fragment. Upper panel contains the list of fragments already validated by HSQC and further tested by TSA. Lower panel, ΔT_m of two non-binder fragments. Fragments were considered

able to stabilize or destabilize the protein if $|\Delta T_m| \geq 0.7\ ^{\circ}C$ already at 3 mM.
ND = not detected (initial fluorescence signal was already too high). NT = not tested
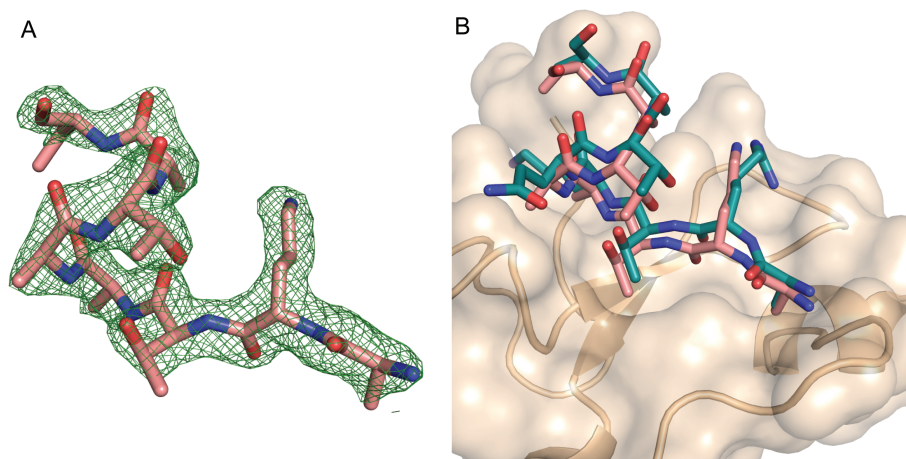*H3 10-mer peptide (ARTKQTARKS)[2] was used as positive control.

Figure S7 BAZ2A in complex with H3 AA mutant peptide. A) $2F_o$-F_c electron density map of the H3 10-mer AA mutant peptide (ARTAATARKS) bound to BAZ2A PHD. Electron density of the peptide is shown till the β-carbon of the residue R8. The last two residues are not visible in the electron density. The $2F_o$-F_c map is in green and contoured at 1 σ. B) Superposition of BAZ2A PHD (wheat surface) in complex with wild-type H3 10-mer (as cyan sticks) and H3 10-mer AA mutant peptide (as pink sticks).
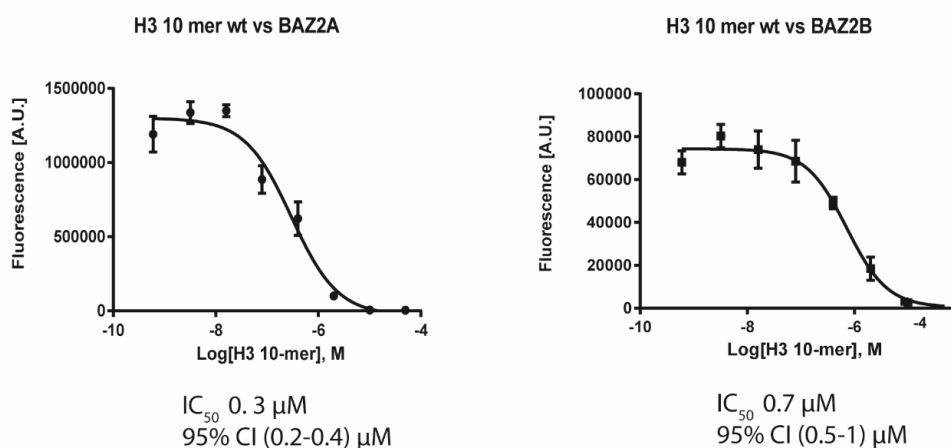

Figure S8 AlphaLISA competition assay.
H3 10-mer peptide (ARTKQTARKS)[2] was used as reference control for the AlphaLISA competition assay with both BAZ2 PHDs. Dose-response curves and IC_{50} were obtained as described in the experimental section and are reported above.
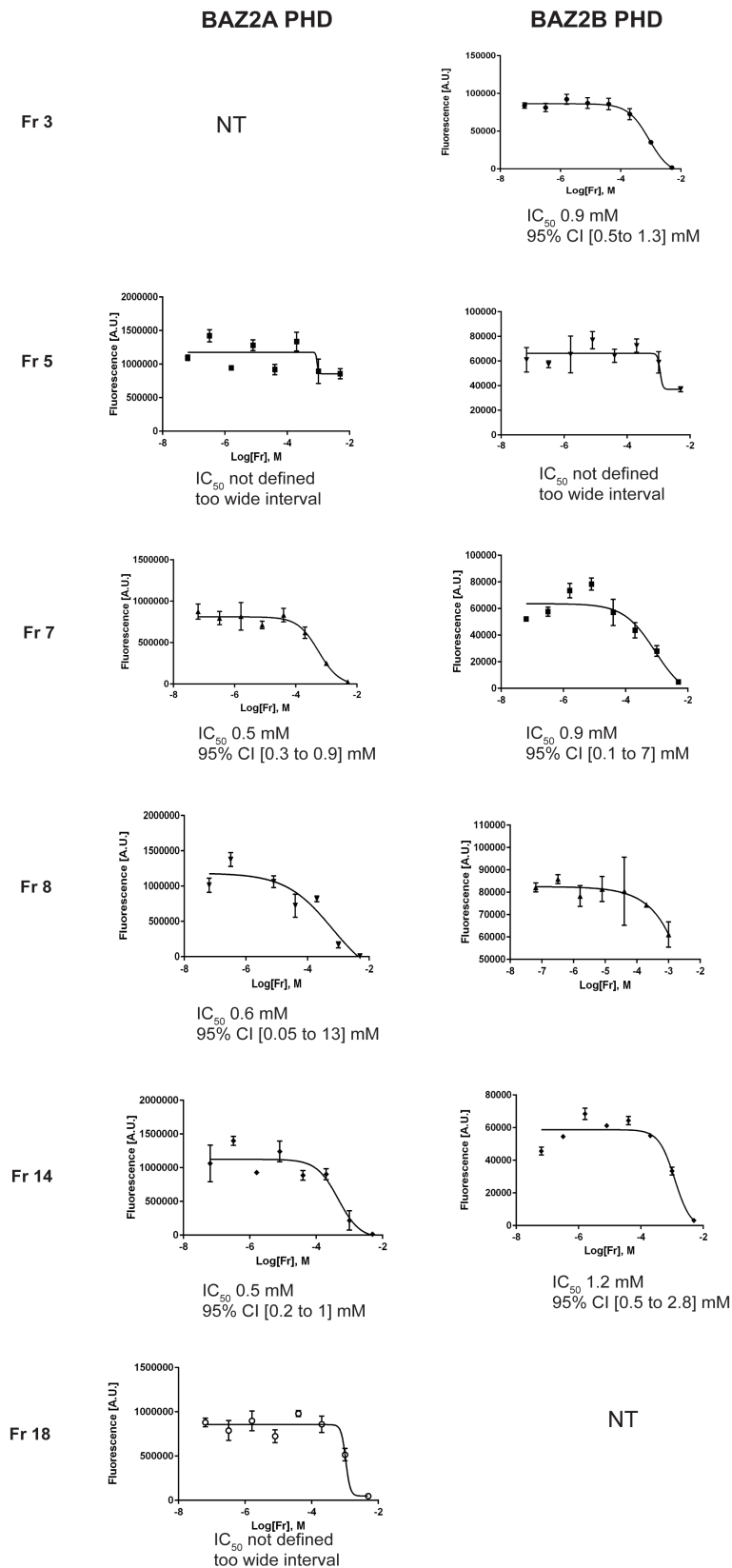
Figure S9. AlphaLISA competition assay with fragments.
HSQC-validated fragments were tested in the AlphaLISA competition assay with both BAZ2 PHDs. Dose-response curves are reported above. IC$_{50}$ were obtained where it was possible to fit the experimental data. NT = not detectable because precipitation of the fragments was

observed during sample preparation. It is interesting to note that Fr**7** and Fr**14** showed displacement of the histone peptide against both proteins, however by NMR CSP analysis they were identified as binder for BAZ2B or BAZ2A only, respectively. Fr**7** was found to bind to the "back pocket" by CSPs, so the ability of this fragment to displace the histone peptide might reflect an allosteric effect.
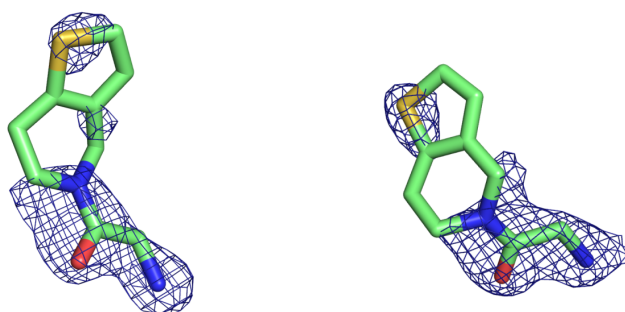

Figure S10. Electron density for Fr19 in complex with BAZ2A PHD.
The $2F_o\text{-}F_c$ electron density map is shown in blue and contoured at 0.9 σ around the Fr**19** ligand bound to chain B (left) and chain C (right).
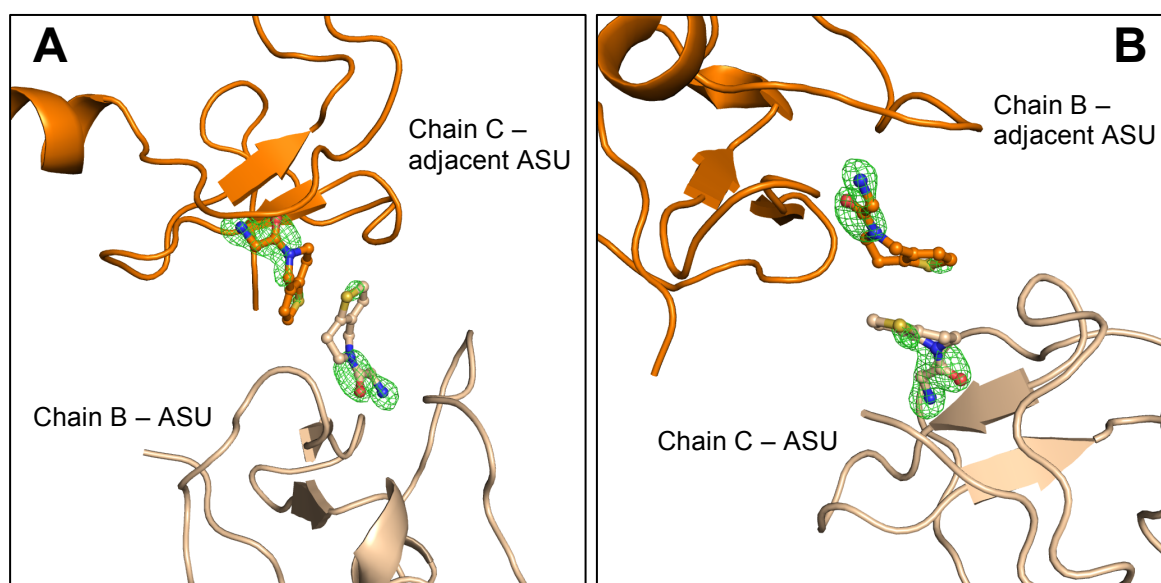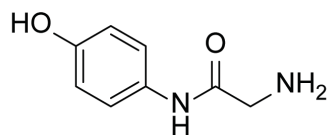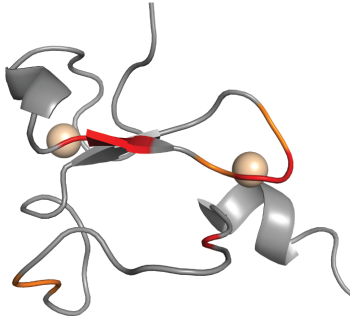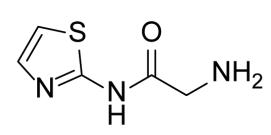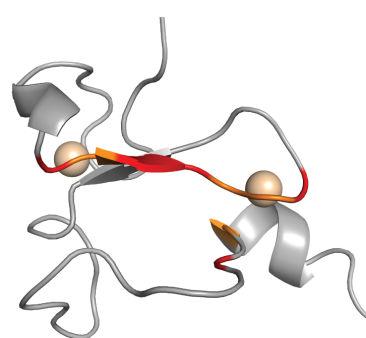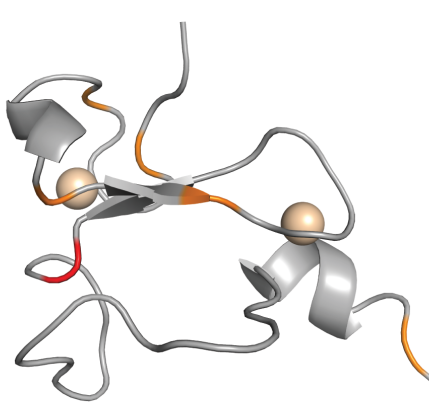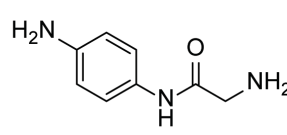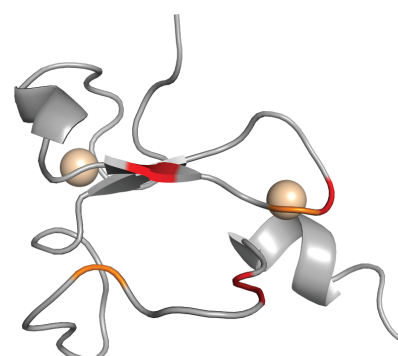

Figure S11. Two binding modes observed for Fr19 with BAZ2A PHD.
Crystallographic packing of BAZ2A PHD induces Fr**19** to adopt two distinct orientations of its 5,6 fused ring, allowing for favourable stacking interactions from neighboring asymmetric unit (ASU) protein chains. The unbiased $F_o\text{-}F_c$ electron density map is shown in green and contoured at 3.0 σ around the bound Fr**19** (shown in stick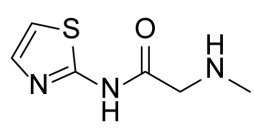 representation). A) Fr**19** and Chain B of the ASU are colored in wheat; Fr**19** and Chain C of the adjacent ASU are colored in orange. B) Fr**19** and Chain C of the ASU are colored in wheat; Fr**19** and Chain B of the adjacent ASU are colored in orange.

A   Fragment   BAZ2A PHD K_D (mM)

Fr 20

11.3 ± 1.4
(LE 0.22)

Fr 21

6.7 ± 1.5
(LE 0.29)

Fr 22

7 ± 3
(LE 0.27)

Fr 23

7.1 ± 1.9
(LE 0.24)

B   Fragment   BAZ2B PHD K_D (mM)

Fr 20

15 ± 3
(LE 0.21)

Fr 21

3.4 ± 0.5
(LE 0.34)

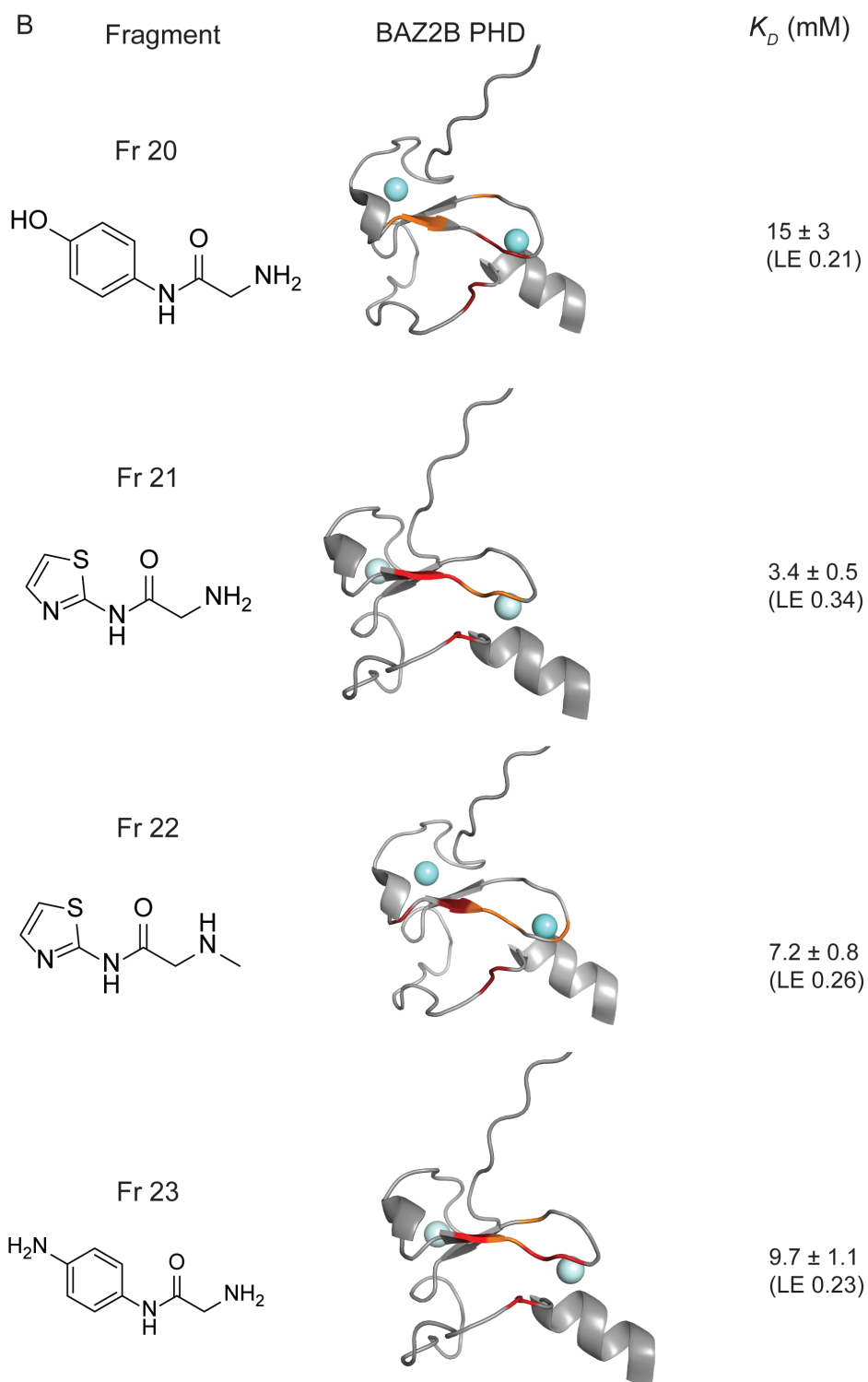Fr 22

7.2 ± 0.8
(LE 0.26)

Fr 23

9.7 ± 1.1
(LE 0.23)

Figure S12. CSPs and K$_D$ estimation for the binding of fragments analogue of Fr19 to BAZ2 PHDs.
K$_D$ values are reported in mM and ligand efficiency in bracket as kcal × mol[-1] × heavy atom[-1].
In panel A, responses are detected for BAZ2A PHD and in panel B, for BAZ2B PHD.

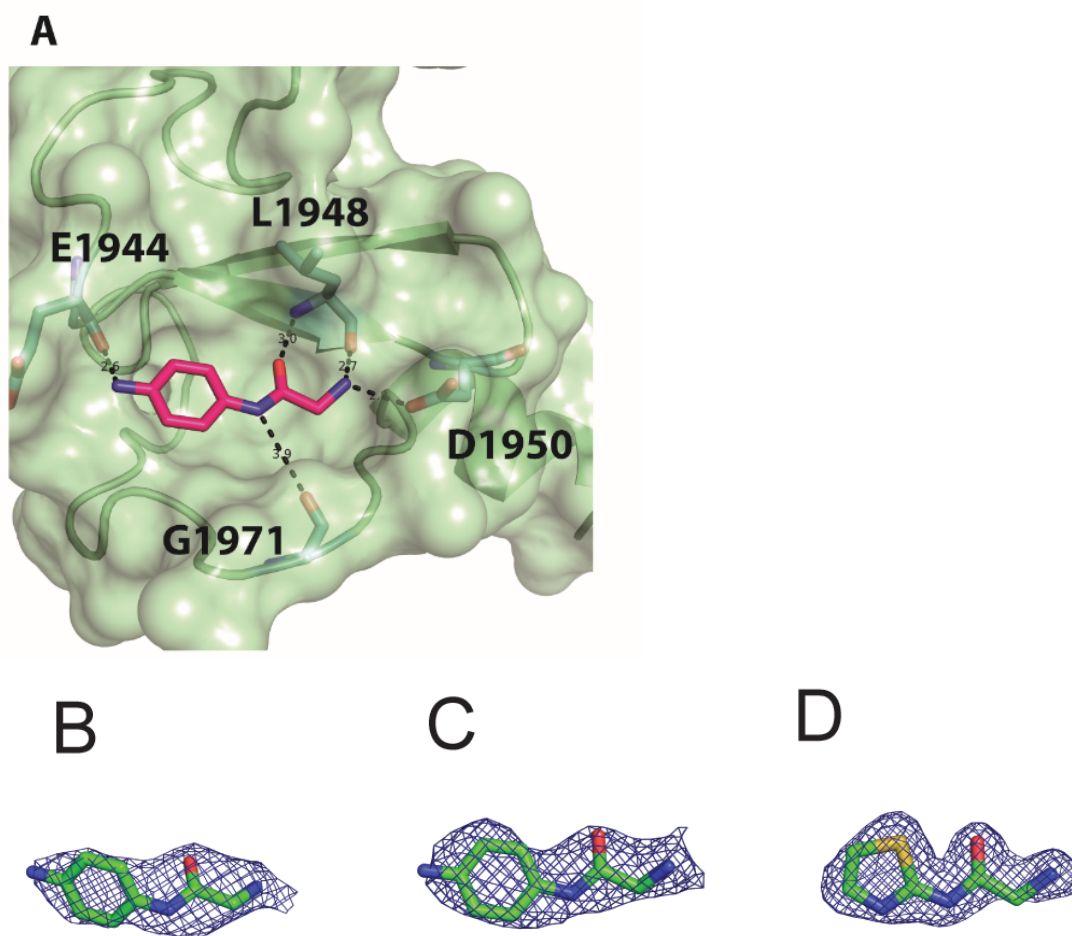**Figure S13. Crystal structures with second series of fragments**

(A) Surface representation of BAZ2B PHD in complex with Fr**23** (sticks, purple carbons). Interacting residues are shown as stick and hydrogen bonds distances are labelled in black.

(B-D) $2F_o$-F_c electron density map is contoured at 1σ. B) Fr**23** bound to BAZ2A PHD; C) Fr**23** bound to BAZ2B PHD; D) Fr**21** bound to BAZ2B PHD.
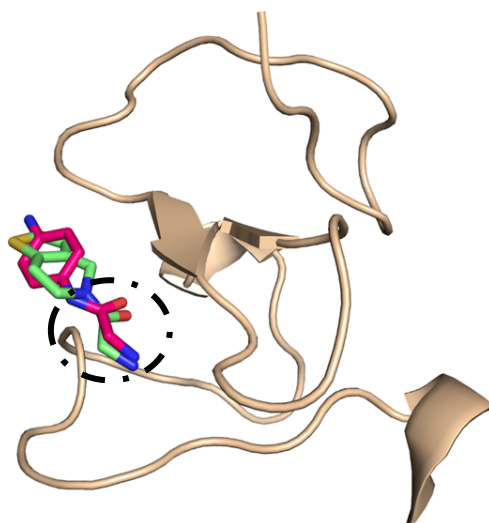
Figure S14. Superposition of BAZ2A PHD in complex with Fr19 (green) and Fr23 (pink).
The superposition is showing that the 2-amino acetamide portion retains the orientation in both fragment-bound structures.

REFERENCES:

[1] Tallant, C., Valentini, E., Fedorov, O., Overvoorde, L., Ferguson, F. M., Filippakopoulos, P., Svergun, D. I., Knapp, S., and Ciulli, A. (2015) Molecular basis of histone tail recognition by human TIP5 PHD finger and bromodomain of the chromatin remodeling complex NoRC, *Structure 23*, 80-92.

[2] Bortoluzzi, A., Amato, A., Lucas, X., Blank, M., and Ciulli, A. (2017) Structural basis of molecular recognition of helical histone H3 tail by PHD finger domains, *The Biochemical journal 474*, 1633-1651.

[3] Williamson, M. P. (2014) Using chemical shift perturbation to characterise ligand binding (vol 73, pg 1, 2013), *Prog Nucl Mag Res Sp 80*, 64-64.

[4] Kabsch, W. (2010) Xds, *Acta Crystallogr D 66*, 125-132.

[5] Kabsch, W. (2010) Integration, scaling, space-group assignment and post-refinement, *Acta Crystallogr D 66*, 133-144.

[6] Battye, T. G., Kontogiannis, L., Johnson, O., Powell, H. R., and Leslie, A. G. (2011) iMOSFLM: a new graphical interface for diffraction-image processing with MOSFLM, *Acta crystallographica. Section D, Biological crystallography 67*, 271-281.

[7] Evans, P. R., and Murshudov, G. N. (2013) How good are my data and what is the resolution?, *Acta Crystallogr D 69*, 1204-1214.

[8] Murshudov, G. N., Vagin, A. A., and Dodson, E. J. (1997) Refinement of macromolecular structures by the maximum-likelihood method, *Acta Crystallogr D 53*, 240-255.

[9] Painter, J., and Merritt, E. A. (2006) TLSMD web server for the generation of multi-group TLS models, *J Appl Crystallogr 39*, 109-111.

[10] Emsley, P., Lohkamp, B., Scott, W. G., and Cowtan, K. (2010) Features and development of Coot, *Acta Crystallogr D 66*, 486-501.

[11] Schuttelkopf, A. W., and van Aalten, D. M. (2004) PRODRG: a tool for high-throughput crystallography of protein-ligand complexes, *Acta crystallographica. Section D, Biological crystallography 60*, 1355-1363.

[12] Chen, V. B., Arendall, W. B., Headd, J. J., Keedy, D. A., Immormino, R. M., Kapral, G. J., Murray, L. W., Richardson, J. S., and Richardson, D. C. (2010) MolProbity: all-atom structure validation for macromolecular crystallography, *Acta Crystallogr D 66*, 12-21.

[13] Brenke, R., Kozakov, D., Chuang, G. Y., Beglov, D., Hall, D., Landon, M. R., Mattos, C., and Vajda, S. (2009) Fragment-based identification of druggable 'hot spots' of proteins using Fourier domain correlation techniques, *Bioinformatics 25*, 621-627.

[14] Kozakov, D., Hall, D. R., Chuang, G. Y., Cencic, R., Brenke, R., Grove, L. E., Beglov, D., Pelletier, J., Whitty, A., and Vajda, S. (2011) Structural conservation of druggable hot spots in protein-protein interfaces, *Proceedings of the National Academy of Sciences of the United States of America 108*, 13528-13533.

[15] Sondergaard, C. R., Olsson, M. H., Rostkowski, M., and Jensen, J. H. (2011) Improved Treatment of Ligands and Coupling Effects in Empirical Calculation and Rationalization of pKa Values, *Journal of chemical theory and computation 7*, 2284-2295.

[16] Olsson, M. H., Sondergaard, C. R., Rostkowski, M., and Jensen, J. H. (2011) PROPKA3: Consistent Treatment of Internal and Surface Residues in Empirical pKa Predictions, *Journal of chemical theory and computation 7*, 525-537.

[17] Sterling, T., and Irwin, J. J. (2015) ZINC 15--Ligand Discovery for Everyone, *Journal of chemical information and modeling 55*, 2324-2337.

[18] Schomburg, K., Ehrlich, H. C., Stierand, K., and Rarey, M. (2010) From structure diagrams to visual chemical patterns, *Journal of chemical information and modeling 50*, 1529-1535.

[19] O'Boyle, N. M., Banck, M., James, C. A., Morley, C., Vandermeersch, T., and Hutchison, G. R. (2011) Open Babel: An open chemical toolbox, *Journal of cheminformatics 3*, 33.

[20] Wallace, A. C., Laskowski, R. A., and Thornton, J. M. (1995) LIGPLOT: a program to generate schematic diagrams of protein-ligand interactions, *Protein engineering 8*, 127-134.

[21] Miller, T. C., Rutherford, T. J., Birchall, K., Chugh, J., Fiedler, M., and Bienz, M. (2014) Competitive binding of a benzimidazole to the histone-binding pocket of the Pygo PHD finger, *ACS chemical biology 9*, 2864-2874.